Photometric stereo using graph cut and M-estimation for a virtual tumulus in the presence of highlights and shadows
Daisuke Miyazaki, Katsushi Ikeuchi,
in Proceedings of Workshop on Applications of Computer Vision in Archaeology,
ACVA 2010, 2010.06

Photometric stereo using graph cut and M-estimation for a virtual tumulus in the presence of highlights and shadows

Daisuke Miyazaki[1] and Katsushi Ikeuchi
Institute of Industrial Science, The University of Tokyo

Abstract

The photometric stereo method is useful for modeling the fine detail of the surface shape of an object. In this paper, we propose a photometric stereo method that uses a graph cut solution. We formulate the photometric stereo problem to the Markov random field problem, and show how to solve the problem by graph cut. The graph cut properly calculates the surface normal and automatically evades the interference of specular reflection. Finally, we show some results when our method is applied to common objects (a diffuse object and a specular object), and to cultural assets, the Segonko Tumulus and Sakurakyo Tumulus.

1. Introduction

It is a benefit to society to allow people to become familiar with precious cultural assets by displaying these objects through the Internet or mobile phones. We can do this by digitally archiving these works, using the photometric stereo method, which preserves the fine detail of the surface shape of such works. We propose a photometric stereo method that can robustly estimate the surface normal and the albedo of these objects and can be applied to objects that involve both diffuse and specular reflection. The key ideas of our algorithm are as follows:

Candidates. Since we take many images under different light conditions, we can choose the data that are not affected by specular reflection and shadow. The problem is how to choose the correct data from candidates [4, 7]. We use graph cut [3, 6, 5] since it can find a solution that is very close to the global minimum.

M-estimation. Some data include specular reflection and shadow; thus, we design a data cost term using M-estimator [10] so that these effects are treated as outliers. We use the Lorentz distribution function instead of the Laplace distribution function [7], since it performs better for removing outliers. M-estimation often causes many local minima; thus, we use graph cut to avoid them.

L2-norm. We use L2-norm instead of L1-norm for the smoothness term since it can represent the smooth surface well. Due to this L2-norm and for other reasons, our smoothness term is not semimetric [3], regular [6], or convex [5]. Since we cannot apply these graph cut methods [3, 6, 5], we use truncated α-expansion.

Truncated α-expansion. We introduce a simple but effective idea that can apply α-expansion [3] to an arbitrarily defined smoothness term. Graph cut is proven to be useful in photometric stereo [4, 13]; thus, we also use it to solve our problem.

1.1. Related work

Various types of methods are proposed to enhance the accuracy of photometric stereo. Miyazaki *et al*. [7] employed the Laplace distribution function as M-estimator to remove the influence of specular reflection. Wu and Tang [14] estimated the surface normal and the albedo robustly using the Expectation-Maximization algorithm. Some methods can be applied to non-Lambertian objects [11, 1, 8]. Chandraker *et al*. [4] chose the non-shadow image using the graph cut method; however, they did not introduce the smoothness constraint for surface normal. Wu *et al*. [13] utilized the smoothness constraint for surface normal. However, their method discretized the surface normal. Unlike Wu's method, our method does not discretize the surface normal; thus, it produces smoother and more natural results. Unlike Chandraker's method, our method utilizes the smoothness constraint for surface normal.

1.2. Overview

The overview of the rest of the paper is as follows. Section 2 explains our graph cut photometric stereo. Section 3 explains our truncated α-expansion. Section 4 shows our results. Finally, in Section 5, we conclude that we have proposed a graph cut photometric stereo that is robust to

[1] Presently with Hiroshima City University

shadow and specularity, and that we have proposed a truncated α-expansion that can be applied to many kinds of problems. We also discuss the disadvantage of our method in this section.

2. Graph cut photometric stereo

In this section, we describe our photometric stereo method. The cost term to be minimized by graph cut is shown in Section 2.1, and the labels used for graph cut are defined in Section 2.2. The overall algorithm is shown in Section 2.3.

2.1. Photometric stereo using graph cut

A min-cut/max-flow algorithm is often called a "graph cut" algorithm. Graph cut is a powerful tool to find the global solution of the Markov random field (MRF) problem [3, 6, 5]. We use the graph cut to choose the best surface normal and albedo from the candidates calculated in Section 2.2. We denote these candidates as label $\mathbf{f}$. The graph cut solves the MRF problem whose data term and smoothness term are described as follows:

$$E_{\mathrm{data}}(\mathbf{f}) = \sum_{p\in\mathcal{P}} D_p(\mathbf{f}_p)\,, \tag{1}$$

$$E_{\mathrm{smooth}}(\mathbf{f}) = \sum_{\{p,q\}\in\mathcal{N}} V_{p,q}(\mathbf{f}_p,\mathbf{f}_q)\,. \tag{2}$$

In order to be robust to outliers, we propose the following data cost term:

$$D_p = \sum_k \mathrm{M_{est}}\left(\mathbf{I}_{k,p} - \mathbf{r}_p\left(\mathbf{n}_p\cdot\mathbf{L}_k\right)\right)\,, \tag{3}$$

where k represents the image number, $\mathbf{I}$ represents the pixel brightness of the input image, $\mathbf{r}$ represents the albedo, $\mathbf{n}$ represents the surface normal, and $\mathbf{L}$ represents the light source direction and its brightness. Here we assume that the light source direction and its brightness are known. $\mathbf{I}$ and $\mathbf{r}$ are three-dimensional vectors which represent RGB channel, and $\mathbf{n}$ and $\mathbf{L}$ are three-dimensional vectors which represent XYZ axes. We apply the graph cut to estimate the surface normal and the albedo alternatively. When calculating the albedo $\mathbf{r}$, we minimize $D_p(\mathbf{r}_p)$ while fixing the surface normal to be the current value. On the other hand, when calculating the surface normal $\mathbf{n}$, we minimize $D_p(\mathbf{n}_p)$ while fixing the albedo to be the current value. In order to avoid the outlier caused by some images, we use M-estimator. Here, we use Lorentz function, $\mathrm{M_{est}}(\mathbf{x}) = \ln(1+\|\mathbf{x}\|^2/2)$, for M-estimator, since it effectively removes outliers.

Many graph cut methods use L1-norm as a smoothness term. L2-norm is more appropriate to express the smoothness; thus, we use the following smoothness term:

$$V_{p,q}(\mathbf{f}_p,\mathbf{f}_q) = \left(\mathbf{f}_p - \mathbf{f}_q\right)^2\,, \tag{4}$$

where p and q represent two neighboring pixels. The smoothness term for albedo and surface normal are $V_{p,q}(\mathbf{r}_p,\mathbf{r}_q)$ and $V_{p,q}(\mathbf{n}_p,\mathbf{n}_q)$, respectively.

We explain the detail of the algorithm in Section 2.3. The definition of the candidates for surface normal and albedo is presented in Section 2.2, and this definition makes the smoothness terms defined above not to be semimetric [3], regular [6], or convex [5]. The conventional graph cut [3, 6, 5] cannot be applied; thus, we use a simple truncated α-expansion algorithm shown in Section 3 to solve the problem.

2.2. Candidates for surface normal

The following candidates of surface normal and albedo are used for the labels when applying the graph cut photometric stereo (Section 2.1). The surface normal can be estimated from three images by using conventional photometric stereo. We denote the number of input images as K. The number of the combination of choosing three images from K images will be:

$${}_K\mathrm{C}_3 = \binom{K}{3} = \frac{K!}{3!(K-3)!} = \frac{1}{6}K(K-1)(K-2)\,. \tag{5}$$

We obtain ${}_K\mathrm{C}_3$ numbers of surface normal and albedo for each pixel [7]. For each pixel, among K brightnesses, some brightnesses are caused by diffuse reflection, while others may be caused by specular reflection or shadow. Therefore, some of the ${}_K\mathrm{C}_3$ surface normals are correctly calculated by three diffuse brightnesses, while others may be wrong. Graph cut chooses the correct surface normal from these candidates. The candidate of surface normal cannot be calculated if the chosen three light sources are coplanar; and in this case, we set a randomly determined surface normal for the candidate so that it can be automatically detected as an outlier.

Since the surface normal is not discretized, this approach is more useful than Wu's [13]. Wu's graph cut photometric stereo [13] divides a unit sphere in 3D space evenly in small regions, and uses the divided triangles' orientation as the candidates for the surface normal. The problem of their approach is the discretization of the surface normal, while we use the surface normal calculated from input images as the candidates.

The problem with our approach is that there would be many candidates. The number of the surface normal increases in cubic proportion; namely, $O({}_K\mathrm{C}_3) = O(K^3)$. Wu *et al*. used 5057 candidates [13]. If we use 33 images or more, the number of the candidates will be 5456 or more, and our approach will be more redundant than Wu's. In the case where the number of input images is 33 or more, we randomly pick 32 or fewer than 32 images and apply our algorithm.

2.3. Algorithm overview

The outline of our algorithm becomes as follows:

1. Calculate ${}_K\mathrm{C}_3$ candidates for surface normal and albedo for each pixel. (Section 2.2)
2. Set initial value for the surface normal and the albedo. (Section 2.3)
3. Using truncated α-expansion, estimate the surface normal by fixing the albedo. (Section 3)
4. Using truncated α-expansion, estimate the albedo by fixing the surface normal. (Section 3)
5. Iterate steps 3–4 until convergence.
6. Height map is calculated from the surface normal.

The cost function we have to minimize is $E_{\mathrm{smooth}} + \lambda E_{\mathrm{data}}$ (Eq. (1) and Eq. (2)), where λ is set manually. An initial value is chosen randomly from the candidates for each pixel.

3. Truncated alpha expansion

Existing methods have restrictions on the smoothness term. The smoothness measure should be one of these: semimetric [3], metric [3], regular [6], or convex [5]. We simply modify the previous method [3] to avoid this problem.

3.1. Two-label Markov random field

The graph cut algorithm minimizes the following cost function:

$$E(f) = \sum_{p \in \mathcal{P}} D_p(f_p) + \sum_{\{p,q\} \in \mathcal{N}} V_{p,q}(f_p, f_q)\,. \qquad (6)$$

If the smoothness term $V(f_p, f_q)$ satisfies the following condition, it is said to be regular [6].

$$V(f_0, f_0) + V(f_1, f_1) \leq V(f_0, f_1) + V(f_1, f_0)\,, \qquad (7)$$

where f_0 and f_1 are certain labels. If there are only two types of labels, f_0 and f_1, and Eq. (7) is satisfied, then Eq. (6) can be globally minimized by setting the edge weight as shown in Fig. 1 [6]. In Fig. 1, the weight of the edge "e" is set as follows.

$$\begin{aligned} &\max(0, V(f_{p,0}, f_{q,1}) + V(f_{p,1}, f_{q,0}) \\ &-V(f_{p,1}, f_{q,1}) - V(f_{p,0}, f_{q,0}))\,. \end{aligned} \qquad (8)$$

If Eq. (7) is satisfied, the truncation does not occur; thus, we can correctly minimize Eq. (6). If Eq. (7) is not satisfied, the edge weight is truncated; we cannot correctly minimize Eq. (6). However, the truncation is necessary since the edge weight should not be negative in order to apply the graph cut. Due to this truncation, the result will often be worse than α-expansion. We discuss the influence of the truncation in the next section.

Algorithm 1 Truncated α-expansion

```
1:  F ≡ {f_p | p ∈ P} ⇐ initial value
2:  success ⇐ 0
3:  for i = 1 to n do
4:     g ⇐ ∅
5:     for all p ∈ P do
6:        g ⇐ g ∪ node(D(α_{p,i}), D(f_p)) // see Fig. 1
7:     end for
8:     for all {p, q} ∈ N do
9:        g ⇐ g ∪ edges(V(α_{p,i}, α_{q,i}), V(α_{p,i}, f_q),
          V(f_p, α_{q,i}), V(f_p, f_q)) // see Fig. 1
10:    end for
11:    F' ⇐ max-flow(g)
12:    if E(F') < E(F) then
13:       F ⇐ F'
14:       success ⇐ 1
15:    end if
16: end for
17: if success = 1 then goto 2
```

3.2. Multi-label Markov random field

In this section, we show an algorithm for the case when there are multiple labels. We use the same iterative framework as for the α-expansion algorithm [3]. Our truncated α-expansion algorithm is shown in Algorithm 1. In this pseudo-code, F represents the labels for each pixel and g represents the graph structure. In line 6 and line 9, we set the weight of the edges as shown in Fig. 1. The number of labels is n (line 3). Line 11 solves the graph cut problem where there are two labels, f_p and $\alpha_{p,i}$, for each pixel. In line 11, we use the min-cut/max-flow algorithm (graph cut algorithm) developed by Boykov and Kolmogorov [2]. The algorithm takes an iterative approach; f_p represents the current label and $\alpha_{p,i}$ represents the chosen label. This iteration is performed until convergence. E represents the error function (Eq. (6)), and line 12 checks the convergence.

One of the differences between our method and the α-expansion algorithm is the truncated edge weight shown in Eq. (8). This modification does not assure theoretically to find the global minimum of the cost function; however, it often produces results good enough to be close to or exactly the same as the global minimum. Our algorithm is guaranteed to always decrease the cost function, and to finally converge.

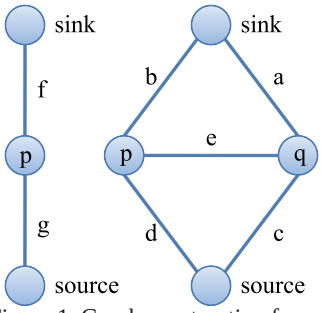

	edge	weight
Smoothness term	a	$V(\alpha_p, \alpha_q) + V(f_p, \alpha_q)$
	b	$V(\alpha_p, \alpha_q) + V(\alpha_p, f_q)$
	c	$V(f_p, f_q) + V(\alpha_p, f_q)$
	d	$V(f_p, f_q) + V(f_p, \alpha_q)$
	e	$\max(0, V(f_p, \alpha_q) + V(\alpha_p, f_q) - V(\alpha_p, \alpha_q) - V(f_p, f_q))$
Data term	f	$D(\alpha_p)$
	g	$D(f_p)$

Figure 1. Graph construction for our graph cut. The nodes p and q are the neighboring nodes. Note that for node p, the weight of the edge between node p and sink, for example, would be $D(\alpha_p) + V(\alpha_p, \alpha_q) + V(\alpha_p, f_q)$.

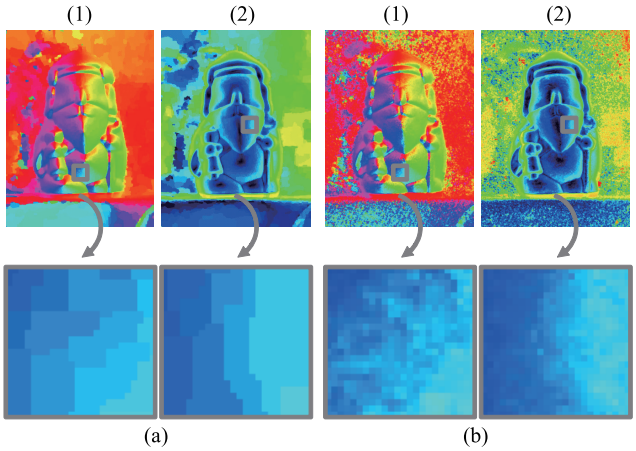

Figure 2. Result of diffuse object, "agastia": (1a) Azimuth angle of surface normal (red: upper direction, blue: left-bottom direction, green: right-bottom direction), result of Wu's photometric stereo (PS); (2a) Zenith angle of surface normal (blue: 0°, red: 90°), Wu's PS; (1b) Azimuth angle, our PS; (2b) Zenith angle, our PS.

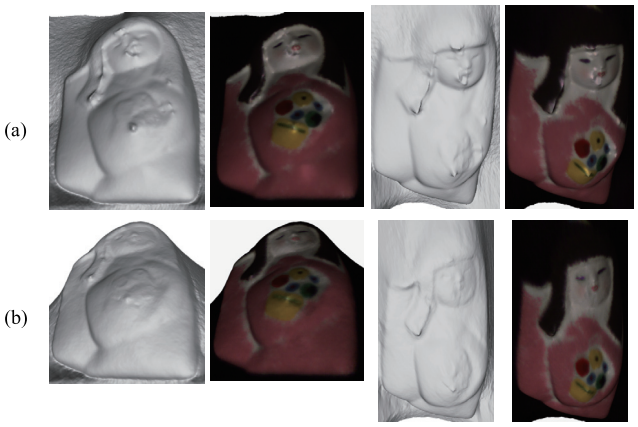

Figure 3. Result of specular object, "ichima": (a) Result of median photometric stereo, (b) Result of our graph cut photometric stereo.

Table 1. Evaluation using RMSE (root mean squared error) of four types of photometric stereo (PS) methods.

	Height RMSE	Normal RMSE
Conventional PS	0.69 cm (90%)	15.22° (148%)
Median PS	0.64 cm (83%)	9.74° (95%)
Wu's graph cut PS	0.61 cm (79%)	10.12° (99%)
Our graph cut PS	0.77 cm (100%)	10.27° (100%)

4. Experimental results

4.1. Qualitative evaluation

First, we use an object which we denote as "agastia," to compare our result with the method proposed by Wu *et al*. [13] (Fig. 2). This object has only diffuse reflection, is made of ceramics, and its design is based on Jurojin, one of Japan's Seven Lucky Gods.

Fig. 2 (b) is the surface normal estimated by using our graph cut photometric stereo. Fig. 2 (a) is the surface normal estimated by the photometric stereo proposed by Wu *et al*. [13]. Although Wu *et al*. use graph cut, they discretize the surface normal; thus, clumsy defects appear in the result.

Next, we use an object which we denote as "ichima," to compare our result with the method proposed by Miyazaki *et al*. [7] (Fig. 3). This object has specular reflection, is made of ceramics, and its design is based on the traditional Japanese Ichimatsu doll.

Fig. 3 (b) is the estimated shape by using our graph cut photometric stereo. Fig. 3 (a) is the shape estimated by the photometric stereo proposed by Miyazaki *et al*. [7]. Our result is less affected by the specular reflection that can be found at the face rendered from the estimated albedo and surface normal.

4.2. Quantitative evaluation

Fig. 4 (e) shows the result of our method applied to the diffuse object "agastia" that is 15 cm tall. We used six input images for this experiment. Fig. 4 (a) is a ground truth obtained by scanning the object by Konica-Minolta VIVID910 laser range sensor. Fig. 4 (b) is the result of conventional

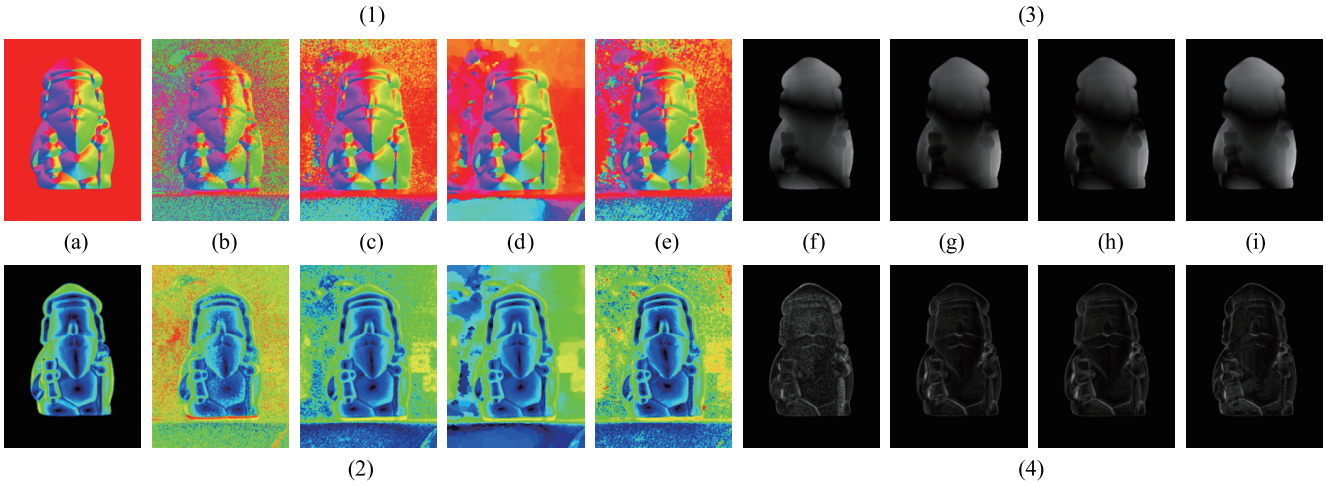

Figure 4. Comparison: (1) Azimuth angle (red: upper direction, blue: left-bottom direction, green: right-bottom direction), (2) Zenith angle (blue: $0°$, red: $90°$), (3) The difference of the height (the brighter the noisier), (4) The difference of the surface normal (the brighter the noisier), (a) True value, (b) The result of conventional PS (photometric stereo), (c) The result of median PS, (d) The result of Wu's graph cut PS, (e) The result of our graph cut PS, (f) The error of conventional PS, (g) The error of median PS, (h) The error of Wu's graph cut PS, (i) The error of our graph cut PS.

PS from three certain input images. Fig. 4 (c) is the result of Miyazaki's method [7]. Fig. 4 (d) is the result of Wu's method [13]. Unfortunately, the comparison in Table 1 shows that the proposed method is slightly worse than the other methods. Since the candidates are fixed, the surface normal is only calculated using three brightnesses. A possible solution would be to perturb the surface normal in order to find a better solution.

The results applied to the diffuse object "buddha" is shown in Fig. 5 (1), and that applied to the specular object "sphere" is shown in Fig. 5 (2). One of the input image out of eight input images is shown in Fig. 5 (a). Fig. 5 (b) is the result of conventional PS from the eight input images. Fig. 5 (c) is the result of Chandraker's method [4]. Fig. 5 (d) is the result of Wu's method [13]. Fig. 5 (e) is the result of Miyazaki's method [7]. Fig. 5 (f) is the result of the proposed method. Unfortunately, the comparison in Table 2 shows that the proposed method is slightly worse than Wu's method. Wu's mehod slightly depends on the data cost term when solving the graph cut, while our method and Chandraker's method depend on the data cost term rather than the smoothness cost; thus, Wu's method produces smoother result than other methods. The reconsideration of the cost terms will be our future work.

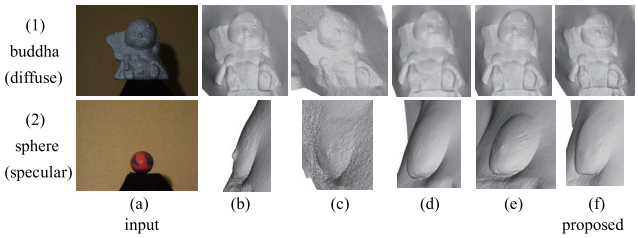

Figure 5. Result of (1) diffuse object, "buddha," and (2) specular object, "sphere": (a) One of the input images, (b) Result of conventional PS (photometric stereo), (c) Result of shadowcut PS, (d) Result of Wu's PS, (e) Result of median PS, (f) Result of our graph cut photometric stereo.

Table 2. Evaluation using RMSE (root mean squared error) of five types of photometric stereo (PS) methods.

	Normal RMSE
Conventional PS	$20.69°$ (149%)
Shadow cut PS	$41.61°$ (300%)
Wu's graph cut PS	$11.13°$ (80%)
Median PS	$13.76°$ (99%)
Our graph cut PS	$13.85°$ (100%)

4.3. Application to a historical cultural asset

In order to verify the usefulness of our method, we applied our method to a historical cultural asset called the Segonko Tumulus, which is located in the Kumamoto prefecture in Japan. The tumulus was built around A.D. 500. Its wall is not only carved but also painted with red, green, and yellow. To preserve the current state of the painting, the tumulus is not open to the public; thus, providing it digitally for common view is important. The measurement system is shown in Fig. 6. The tumulus is a very small chamber, and only one or two people can go inside (Fig. 7). The input images are shown in Fig. 8 (a). The images rendered from the

Figure 6. Measurement system “Photometric Wing” used for the tumuluses.

Figure 7. The measurement system capturing images inside the small cave.

Figure 8. (a) Input images, and (b) rendered images of Segonko Tumulus.

estimated albedo and the surface normal are shown in Fig. 8 (b). A typhoon attacked us on the first day of our scanning mission. We captured the images another day; however, the wall was wet. The specularities occurred on the surface of the wall, but our method was not affected by such specularities. Note that the specularities are removed in Fig. 8 (b). The result of the shape is shown in Fig. 9. We can clearly detect the hole in the center of the concentric circles, and thus we were able to give evidence to the opinion of the archaeologist that the circle was carved by using compasses.

We also applied our method to a historical cultural asset called the Sakurakyo Tumulus, which is located in the

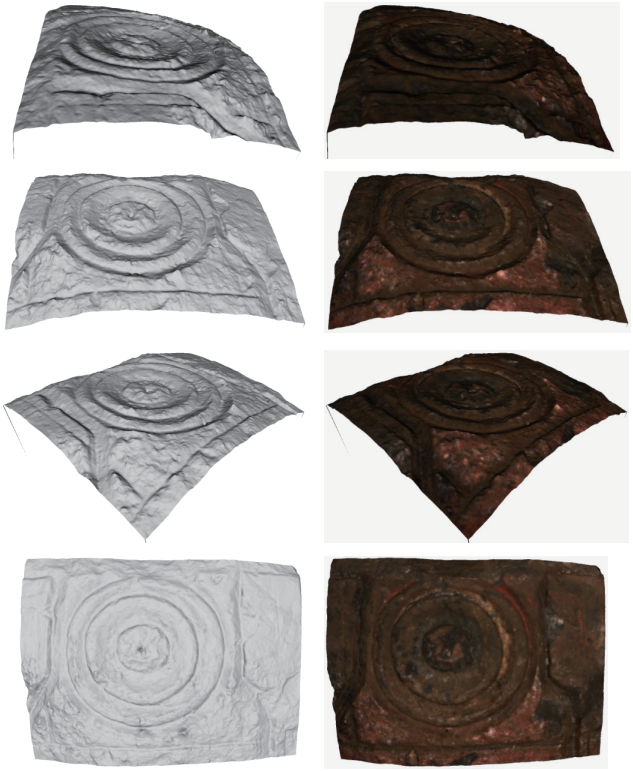

Figure 9. Result of applying our method to a segment of the Segonko Tumulus, constructed around 500 A.D. This experiment confirmed that compasses were used to create the concentric circles.

Fukuoka prefecture in Japan (Fig. 10 (a)). The tumulus was built around the second half of the sixth century. Its wall is not only carved with continuous triangle shape but also painted with red, green, and yellow. To preserve the current state of the painting, the tumulus is not open to the public; thus, providing it digitally for common view is important. We used the same measurement system as used in the Segonko Tumulus. The chamber of the Sakurakyo Tumulus is as small as that of the Segonko Tumulus. The result of the shape is shown in Fig. 10 (b). We can clearly detect the triangle shape of the carving, which are hardly recognizable in the photos.

5. Conclusion

In this paper, we propose a photometric stereo that is useful for digitizing the fine detail of cultural assets. Our graph cut photometric stereo is robust to shadow and specular reflection.

The problem of calculating candidates for surface normal is the computation time, since it needs $O(N^3)$. However, our algorithm is still robust for a small number of images; thus, our method can be applied to a small number of

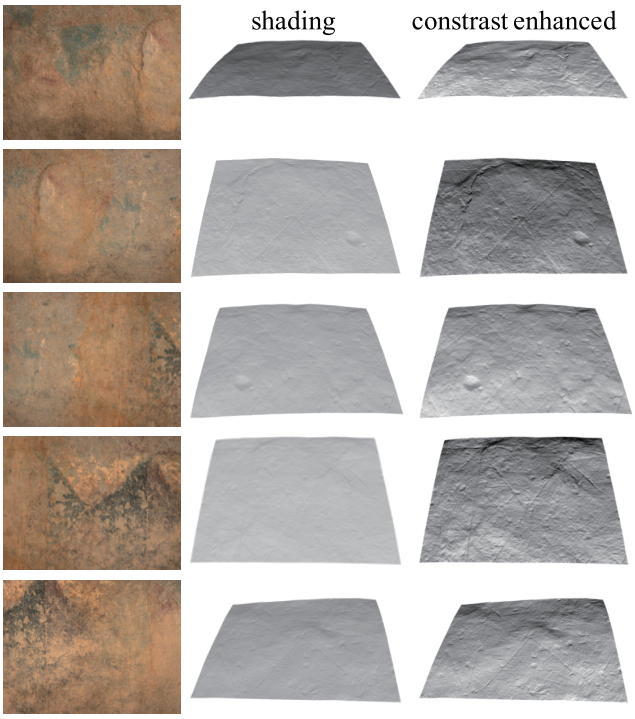

Figure 10. The wall of the Sakurakyo Tumulus. (a) Input images, and (b) estimated shape.

images.

In this paper, the light source is assumed to be an infinite far point light source (directional light source), and extending it to a point light source could be valuable future work.

Acknowledgement

This research was supported in part by the Ministry of Education, Culture, Sports, Science and Technology under the Leading Project, "Development of High Fidelity Digitization Software for Large-Scale and Intangible Cultural Assets." SONY XCD-X710CR, FUJINON lens, TECHNO SCOPE CFW-46, Chori Imaging VFS-42, SHARP laptop PC, LPL lamp holder, SLIK and ETSUMI camera plates, Edmund Optics articulated arms, Velbon tripods, Labsphere white reference, and TOKYU HANDS specular sphere were used in the experiment. KONICA MINOLTA VIVID 910, the alignment software developed by Oishi *et al*. [9], and the camera calibration [12] software developed by Ryo Kurazume, Hiroki Unten, Ryo Ohkubo, Fujitsu Ltd., and Atsuhiko Banno, were used in the evaluation. Tetsuya Kakuta provided the geometric dome data which was used, in part, in one of our softwares. The source code of max-flow algorithm was provided by Boykov and Kolmogorov [2]. The tutorial presented by Hiroshi Ishikawa helped the authors understand the graph cut algorithm. The launch of this research was stimulated by the work done by Koichi Ogawara, Yasuhide Okamoto, and our previous work [7]. The measurement of "Segonko Tumulus" was supported by Nobuaki Kuchitsu, Kumamoto Prefectural Board of Education, and Toppan Printing Co., Ltd. The measurement of "Sakurakyo Tumulus" was supported by Nobuaki Kuchitsu, Munakata city, and Toppan Printing Co., Ltd. They also thank anonymous reviewers for their careful reviews of the paper.

References

[1] N. Alldrin, T. Zickler, and D. Kriegman, "Photometric stereo with non-parametric and spatially-varying reflectance," in *Proc. IEEE Computer Vision and Pattern Recognition*, 2008.

[2] Y. Boykov and V. Kolmogorov, "An experimental comparison of min-cut/max-flow algorithms for energy minimization in vision," *IEEE Trans. Pattern Analysis and Machine Intelligence*, vol. 26, no. 9, pp. 1124–1137, 2004.

[3] Y. Boykov, O. Veksler, and R. Zabih, "Fast approximate energy minimizaiton via graph cuts," *IEEE Trans. Pattern Analysis and Machine Intelligence*, vol. 23, no. 11, pp. 1222–1239, 2001.

[4] M. Chandraker, S. Agarwal, and D. Kriegman, "Shadowcuts: photometric stereo with shadows," in *Proc. IEEE Computer Vision and Pattern Recognition*, 2007.

[5] H. Ishikawa, "Exact optimization for Markov random fields with convex priors," *IEEE Trans. Pattern Analysis and Machine Intelligence*, vol. 25, no. 10, pp. 1333–1336, 2003.

[6] V. Kolmogorov and R. Zabih, "What energy functions can be minimized via graph cuts?," *IEEE Trans. Pattern Analysis and Machine Intelligence*, vol. 26, no. 2, pp. 147–159, 2004.

[7] D. Miyazaki, K. Hara, and K. Ikeuchi, "Median photometric stereo as applied to the Segonko tumulus and museum objects," *International Journal of Computer Vision*, vol. 86, no. 2–3, pp. 229–242, 2010.

[8] S. K. Nayar, K. Ikeuchi, and T. Kanade, "Determining shape and reflectance of hybrid surface by photometric sampling," *IEEE Trans. Robotics and Automation*, vol. 6, no. 4, pp. 418–431, 1990.

[9] T. Oishi, A. Nakazawa, R. Kurazume, and K. Ikeuchi, "Fast simultaneous alignment of multiple range images using index images," in *Proceedings of International Conference on 3-D Digital Imaging and Modeling*, pp. 476–483, 2005.

[10] W. H. Press, S. A. Teukolsky, W. T. Vetterling, and B. P. Flannery, *Numerical recipes in C: the art of scientific computing*, p. 994, Cambridge University Press, 1992.

[11] P. Tan, S. P. Mallick, L. Quan, D. J. Kriegman, and T. Zickler, "Isotropy, reciprocity and the generalized bas-relief ambiguity," in *Proc. IEEE Computer Vision and Pattern Recognition*, 2007.

[12] R. Y. Tsai, "An efficient and accurate camera calibration technique for 3D machine vision," in *Proceedings of IEEE Computer Society Conference on Computer Vision and Pattern Recognition*, pp. 364–374, 1986.

[13] T. P. Wu, K. L. Tang, C. K. Tang, and T. T. Wong, "Dense photometric stereo: a Markov random field approach," *IEEE Trans. Pattern Analysis and Machine Intelligence*, vol. 28, no. 11, pp. 1830–1846, 2006.

earlier: T. P. Wu and C. K. Tang, "Dense photometric stereo using a mirror sphere and graph cut," in *Proc. IEEE Computer Vision and Pattern Recognition*, pp. 140–147, 2005.

earlier: K. Tang, C. Tang, and T. Wong, "Dense photometric stereo using tensorial belief propagation," in *Proc. IEEE Computer Vision and Pattern Recognition*, pp. 132–139, 2005.

[14] T.-P. Wu and C.-K. Tang, "Photometric stereo via expectation maximization," *IEEE Trans. Pattern Analysis and Machine Intelligence*, vol. 32, no. 3, pp. 546–560, 2010.